journal

J. Am. Ceram. Soc., 73 [4] 1026–33 (1990)

Stress-Biased Anisotropic Microcracking in Zirconia Polycrystals

Patricio E. Reyes-Morel*† and I-Wei Chen*

Department of Materials Science and Engineering, University of Michigan, Ann Arbor, Michigan 48109–2136

Anisotropic elastic response of microcracked bodies has been studied using transformation-toughened Mg-PSZ and Ce-TZP as model materials. These zirconias have been previously deformed in triaxial compression to effect various extents of phase transformation. Microcracks were found to align with the compression axis and their normalized density increases linearly with the extent of transformation plasticity. The measured elastic constants are anisotropic and well described by an elasticity theory. An additional anomalous elastic anisotropy was also found in Ce-TZP due to a transformation texture of both the remaining tetragonal phase and the newly formed monoclinic phase. The terminal crack density $\omega = Na^3$, where N is the number of cracks per unit volume and a is the crack radius, reaches 0.05 in Mg-PSZ and 0.1 in Ce-TZP at the completion of transformation plasticity. [Key words: microcracking, partially stabilized zirconia, elastic constants, plasticity, phase transformations.]

I. Introduction

MICROCRACKING is a common phenomenon in ceramics. One well-studied example is microcracking due to anisotropic thermal expansion.[1,2] In polycrystals without a texture, thermally induced microcracks are randomly distributed along grain boundaries. The resultant weakening of elastic stiffness in a randomly cracked body has been theoretically analyzed.[3,4] The latter result has been widely quoted in ceramic and mechanics literature. Microcracks also form as a byproduct of deformation. The distribution of microcracks induced by deformation, however, is distinctly anisotropic. This is well-known in rock mechanics studies in which uniaxial and triaxial compression is commonly employed[5] and in creep fracture studies in which uniaxial tension is of great interest.[6] In all such cases, microcracks extending along grain boundaries are found to be preferentially aligned perpendicular to the maximal principal stress axis.

Anisotropic microcracks associated with transformation plasticity are of a similar nature.[7] This is illustrated in Fig. 1, which depicts the cracking mechanism under a distant uniaxial loading. The primary mechanical force responsible for crack formation stems from the shear component of phase transformation which produces a wedge opening at the grain boundary. The distant stress biases both the direction of shear and the direction of crack propagation in such a way as to favor crack formation perpendicular to the axis of the maximal principal stress. This is essentially the Zener–Stroh mechanism[8,9] well-known in fracture. Such intergranular microcracks are initially limited in length to one grain size for crystallographic reasons. As transformation plasticity proceeds, the density of microcracks increases. Micrographs of uniaxially compressed, coarse-grained magnesia-partially-stabilized zirconia (Mg-PSZ) have been obtained which support the above picture.[7]

Microcracking during deformation affects the mechanical response of the deformed body in several distinct ways. First, the preferential orientation of microcracks causes anisotropy in the elastic properties and a drastic weakening in certain directions and under certain loading conditions.[10] Second, a nonlinear elastic strain increment is produced due to the changing compliance as a result of crack formation.[5,11] Third, any residual crack-opening displacement or frictional surface sliding movement contributes additionally to the apparent plasticity.[5,11] Like the elastic response, the partition of microcrack plasticity is inherently anisotropic. Therefore, many possible fracture mechanics effects, such as crack shielding and residual stresses in monotonic[12] and cyclic loading,[13] can be profoundly modified by the anisotropy of such elastic and plastic properties. A sound understanding of the mechanical response of anisotropically cracked ceramics is thus desirable.

The present paper is devoted to the study of the elastic properties of such objects using two transformation-toughened zirconias as model materials. To our knowledge such studies have not been reported in the literature, probably because laboratory-sized specimens with a controlled, uniform, but anisotropic, distribution of microcracks cannot be generated easily. (Most rock mechanics studies use natural rocks which are very coarse-grained so that crack distribution is not homogeneous. Thermally cracked ceramics, on the other hand, do not have the requisite anisotropy in crack distribution.) We have compared our data with the theoretical predictions and found them in good agreement. As a byproduct of this study, we have also obtained some new insight into microscopic characteristics of transformation plasticity,[7] including a direct assessment of the damage parameter and the consequence of transformation texture on elastic properties. The quantification of the crack density associated with transformation plasticity is especially worth noting, for such a task has proved difficult in the past primarily because of crack closure under the compressive residual stress following the dilatant transformation. Although transmission electron microscopy has provided some quantitative information regarding microcracks, such a technique may suffer from artifacts due to the altered stress state in the thin foil and the lack of statistical significance in general. By studying the anisotropic elastic response of microcracked macroscopic bodies, we hope we have provided the first definitive measurements of microcrack densities associated with transformation plasticity.

K. Faber—contributing editor

Manuscript No. 198255. Received July 13, 1989; approved October 25, 1989.

Based on the Ph.D. thesis submitted by P. E. Reyes-Morel to the Massachusetts Institute of Technology, June 1986.

Supported by the Chilean Government.

*Member, American Ceramic Society.

†Current address: Comisión Chilena de Energía Nuclear, Santiago, Chile.

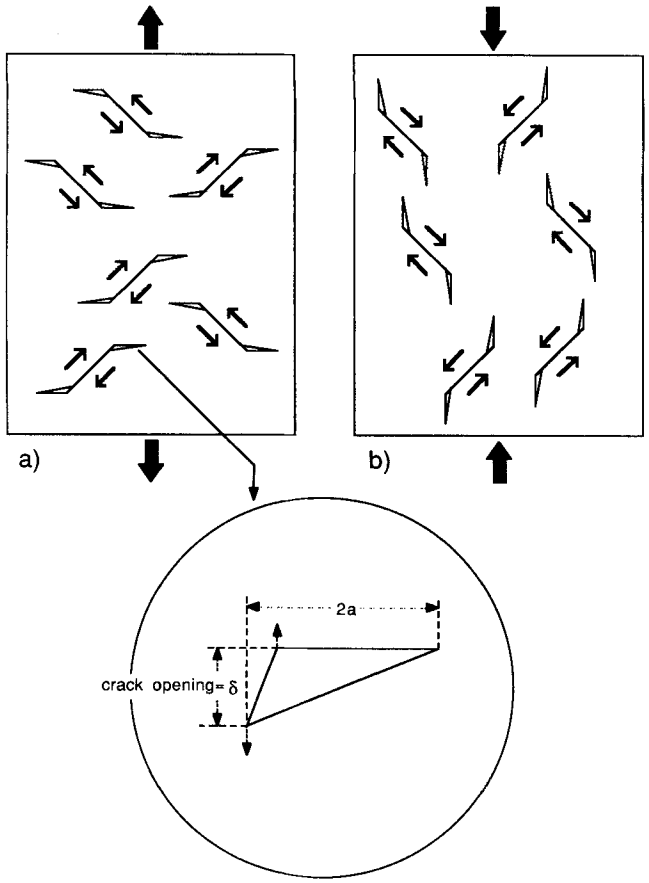

Fig. 1. Schematic of microcracks formed when shear bands intercept grain boundaries: (a) microcracks perpendicular to tensile stress axis, (b) microcracks parallel to compression stress axis.

II. Theory of Elastic Moduli of a Microcracked Body

(1) Stiffness Matrix

The generalized relationship for Hooke's law is represented by

$$\varepsilon = \mathbf{s}\sigma$$

or

$$\sigma = \mathbf{c}\varepsilon \tag{1}$$

where **s** and **c** are matrices of proportionality constants called compliance and stiffness, respectively. Using a matrix notation, in which the indices run from 1 to 6, the relation takes the form

$$\varepsilon_i = s_{ij}\sigma_j$$

or

$$\sigma_i = c_{ij}\varepsilon_j \tag{2}$$

Here the indices are ordered with reference to the Cartesian coordinate (x, y, z) of Fig. 2 in the following sequence: xx, yy, zz, yz, zx, xy.

We assume that the uncracked solid is elastically isotropic. Under axially symmetric deformation it degrades to possess only transverse anisotropy as microcracking takes place. A material of such symmetry behaves like a hexagonal crystal in symmetry-related properties. For example, waves transmitted along the unique axis and an axis perpendicular to it will have different wave velocities, while waves along any two transverse axes are indistinguishable.

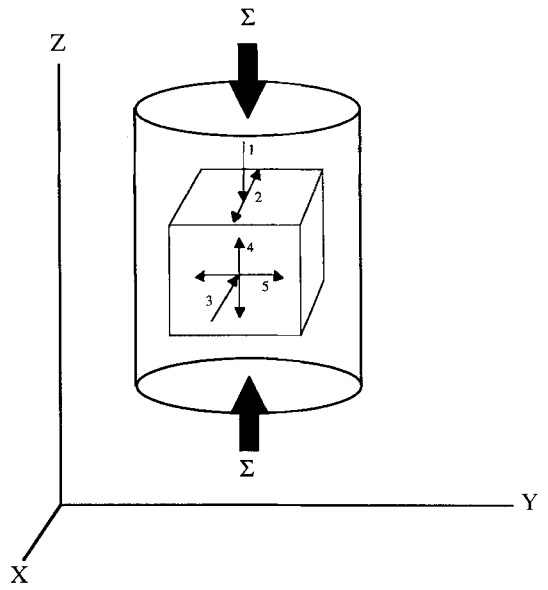

Fig. 2. Cylindrical compression specimen with the compression axis designated as the z axis. Also shown is a cube used for ultrasonic measurements. A single-sided arrow indicates the polarization vector of a longitudinal wave, while a double-sided arrow indicates the polarization vector of a transverse wave with a normal incidence onto the cube surface.

Five elastic constants are independent for a material with transverse isotropy

$$c_{11} = c_{22};\ c_{12};\ c_{13} = c_{23};\ c_{33};$$
$$c_{44} = c_{55};\ c_{66} = (c_{11} - c_{12})/2 \tag{3}$$

Thus, the stiffness matrix takes the form

$$\begin{matrix} c_{11} & c_{12} & c_{13} & 0 & 0 & 0 \\ c_{12} & c_{11} & c_{13} & 0 & 0 & 0 \\ c_{13} & c_{13} & c_{33} & 0 & 0 & 0 \\ 0 & 0 & 0 & c_{44} & 0 & 0 \\ 0 & 0 & 0 & 0 & c_{44} & 0 \\ 0 & 0 & 0 & 0 & 0 & (c_{11} - c_{12})/2 \end{matrix} \tag{4}$$

(2) Crack Density Dependence of Stiffness

In the present case pertaining to compression as shown in Fig. 1(b), we may assume that cracks are oriented along the [001] direction and that their distribution is otherwise transversely symmetric with respect to the same. A crack density is now defined. It is the (normalized) crack density, Na^3, and denoted by ω. Here N is the number of cracks per unit volume and a is the crack radius. Only circular cracks are considered. In the limit of small ω, it is obvious that all the stiffness constants decrease linearly with ω in the form of

$$c_{ij}(\omega) = c_{ij}(0)\,(1 + \Delta_{ij}\omega) \tag{5}$$

where Δ_{ij} is a matrix to be defined later. In the above, $c_{ij}(0)$ is the stiffness matrix component of the uncracked reference solid and $c_{ij}(\omega)$ is the corresponding property of the cracked solid at a crack density ω. Hoenig[10] has considered the present problem of an axially cracked body and derived the compliance matrix s_{ij}. If we focus on the dilute crack density limit of his result, and convert it to the compliance matrix with lengthy but straightforward algebra, we obtain the linear form cast above in Eq. (5), where

$$\Delta_{11} = \Delta_{22} = [2(8 - 3\nu)]/[3(2 - \nu)] - \Delta \tag{6a}$$
$$\Delta_{33} = [4(8 - 3\nu - \nu^2)]/[3(2 - \nu)] - \Delta \tag{6b}$$

$$\Delta_{12} = \Delta_{21} = [2(1 - \nu)]/[3(2 - \nu)] - \Delta \quad (6c)$$

$$\Delta_{13} = \Delta_{23} = \Delta_{32} = \Delta_{31}$$
$$= [2(1 - \nu)(4 - \nu)]/[3(2 - \nu)] - \Delta \quad (6d)$$

$$\Delta_{44} = \Delta_{55} = -[8(1 - \nu)]/[3(2 - \nu)] \quad (6e)$$

$$\Delta_{66} = -[4(1 - \nu)(4 - \nu)]/[3(2 - \nu)] \quad (6f)$$

with

$$\Delta = [4(1 - \nu)(8 - 11\nu + 2\nu^2)]/[3(1 - 2\nu)(2 - \nu)] \quad (7)$$

and ν being the Poisson's ratio. (In the derivation, we have used Eqs. 3.7, 3.8, 3.24, 3.26, 3.29, and 3.30 in Hoenig's paper.[10] With the expressions for the influence coefficients d_1, d_2, and d_3 used thereof, obtained from a previous study of Hoenig's, his Ref. 9, we obtained an explicit form of the compliance matrix which was then inverted.)

The mathematical limit of dilute crack density corresponds to the physical situation in which microcracks are not interacting. This is because Hoenig's derivation began with the fundamental solution of a single crack, of any orientation, in an infinite isotropic elastic solid. Such solutions were then superimposed onto each other according to the requisite crack density and symmetry to arrive at the compliance matrix. This procedure is valid as long as the crack density is sufficiently low so that their interactions are negligible. At higher densities, this assumption can still be justified as long as a favorable comparison between the experimental and the above prediction is demonstrated. This turns out to be the case in our study. Eventually, crack interactions may be approximately accounted for by replacing the linear relation with an exponential one

$$c_{ij}(\omega) = c_{ij}(0) \exp(\Delta_{ij}\omega) \quad (8)$$

based on an incremental self-consistent method reviewed elsewhere.[14] Such a technique may be used instead of the numerically more involved method found in Hoenig's work,[4,10] although further experimental studies on specimens of very high crack densities are required to test both predictions.

The above theory is the basis for understanding the elastic response of a microcracked solid of the type shown in Fig. 1(b). To provide a graphical illustration of the effect of microcracking on stiffness, we let $\nu = 0.3$, which is typical for zirconia ceramics, and plot $c_{ij}(\omega)/c_{ij}(0)$ using Eqs. (6) to (8). As shown in Fig. 3, the normalized elastic stiffness decreases in the following order: c_{44}, c_{33}, c_{66}, c_{11}, c_{13}, c_{12}, due to microcracking along the [001] axis. At small ω, these stiffness constants decrease linearly as expected from Eq. (5). The exponential curvature becomes significant at large ω. The physical meaning of the relative decrease of the stiffness components will become clear in Section II(4).

(3) Renormalization of Stiffness

To apply the above result to transformation-induced microcracking, it is important to recognize that the elastic moduli of the product phase may be different from the parent phase. That is, c_{ij}°, the stiffness of the undeformed, uncracked solid, may be different from $c_{ij}(0)$, the stiffness of the reference solid to which microcracks are introduced. Here the reference solid should be identified as the uncracked but deformed and thus transformed polycrystalline assemblage. An independent measurement of the moduli of the transformed but uncracked solid, however, is not feasible because microcracking is a necessary byproduct of displasive transformation in brittle ceramics. Such cracks can be closed only under a very high hydrostatic pressure, but the latter, in turn, causes reverse transformation[15] as we found experimentally. One can, nevertheless, overcome the above complication by using a renormalization procedure described below.

First, let $\mathbf{C}$ denote a normalized stiffness matrix

$$C_{ij} = c_{ij}(\omega)/c_{ij}(0) \quad (9)$$

We then define, for small ω, a renormalized quantity $\mathbf{C}^*$

$$C_{ij}^* = C_{ij}/C_{66} = 1 + (\Delta_{ij} - \Delta_{66})\omega \quad (10)$$

Thus, C_{ij}^* is always independent of the moduli of the uncracked matter. In the above, we have chosen C_{66} as the constant for the second normalization, although this choice is entirely arbitrary and all other stiffness constants may be used for this purpose as well. If we further assume

$$c_{ij}(0)/c_{ij}^{\circ} = \text{constant independent of } ij \quad (11)$$

then we find that the first normalization could have been carried out with respect to c_{ij}° without affecting the final result obtained after the second normalization. It should be noted that the condition for Eq. (11) is actually not very restrictive. Specifically, one can easily prove that it is satisfied among all *isotropic* solids of the *same Poisson's ratio.* (This is a direct consequence of the fact that an isotropic solid has only two independent elastic constants which are now fixed by Poisson's ratio and the constant of Eq. (11).) Since Poisson's ratios for zirconia ceramics are nearly identical, ca. 0.3, it is satisfied in essentially all transformation-toughened polycrystals which do not have a strong texture.

Based on the above reasoning, the stiffness data reported in this study will be renormalized using the values of undeformed, untransformed zirconia. This is the case for Mg-PSZ, since the transformed Mg-PSZ polycrystal still largely retains random grain orientations. For later reference, we list the constants in Eq. (10):

$$\Delta_{11} - \Delta_{66} = -[2\nu(7 - \nu)]/[3(2 - \nu)(1 - \nu)] \quad (12a)$$

$$\Delta_{33} - \Delta_{66} =$$
$$[4(4 - 13\nu + 3\nu^2 + 2\nu^3)]/[3(2 - \nu)(1 - 2\nu)] \quad (12b)$$

$$\Delta_{12} - \Delta_{66} =$$
$$-[2(7 - 2\nu)(1 - \nu)]/[3(2 - \nu)(1 - 2\nu)] \quad (12c)$$

$$\Delta_{13} - \Delta_{66} =$$
$$-[2(4 + 5\nu - 2\nu^2)(1 - \nu)]/[3(2 - \nu)(1 - 2\nu)] \quad (12d)$$

$$\Delta_{44} - \Delta_{66} = 4(1 - \nu)/3 \quad (12e)$$

(4) E and ν in Axial Deformation

In the generalized Hooke's law under a uniaxial stress state along [001], Young's modulus is defined as

$$E \equiv \sigma_3/\varepsilon_3 = (s_{33})^{-1} \quad (13)$$

It turns out that E is unchanged by axial microcracks. Similarly, Poisson's ratio, defined as the proportionality constant between $-\varepsilon_1$ and ε_3

$$\nu = -\varepsilon_1/\varepsilon_3 = -s_{13}/s_{33} \quad (14)$$

is also unchanged. These two are the only constants, among the five independent ones, that are not affected by axial cracks. The physical meaning of these two results can be easily appreciated by viewing the extreme case of a solid containing parallel "long" cracks. When deformed in the axial direction parallel to the long cracks, the solid behaves as a bundle of parallel columns, still fully capable of carrying loads, and has no transverse interaction other than a uniform Poisson contraction/expansion. In such cases, its elastic response in terms of E and ν in the axial deformation is unaffected by the existence of cracks.

The above picture can also be used to understand qualitatively the relative magnitude of weakening of C_{44}, C_{33}, C_{66}, C_{11}, C_{13}, and C_{12}, shown previously. For example, C_{12} is severely weakened by the loss of shear stiffness across the crack plane, while C_{33} is only slightly weakened because the columns can still support load in the axial direction. These predictions will be specifically verified in the following experimental study.

III. Experimental Procedure

(1) Materials

Materials used in the present study were an Mg-PSZ and a Ce-TZP which have been extensively characterized for their transformation plasticity.[15-18] Essentially, Mg-PSZ (containing 8 mol% MgO) is a coarse-grained cubic zirconia of 50-μm grain size with tetragonal precipitates occupying 33% of the total volume, whereas Ce-TZP (containing 12 mol% CeO_2) is a fine-grained tetragonal zirconia of 1.2-μm grain size. These materials were deformed in uniaxial compression with a superimposed pressure to effect transformation to various extents. The specimens used for compression were cylinders of 12-mm diameter and 24-mm height. As reported elsewhere,[7] such test conditions, under which the uniaxial and triaxial stresses are independently controlled, are especially suited for the study of transformation plasticity which has a dilatational component. For the purpose of the present work the confining pressure serves to stabilize the microcrack propagation to allow a high density of microcracks to fully develop uniformly in a macroscopic volume, thus facilitating subsequent characterization of elastic properties. To monitor deformation and the extent of transformation, axial and radial strains were measured using strain gauges which, in turn, provided the volumetric strains. The latter was directly converted to the fraction of phase transformation using the molar volume increase of 0.044 from tetragonal to monoclinic phases. The fraction of phase transformation, denoted by ϕ, will be used as a state variable for the transformed materials. Thus, when $\phi = 1$, the volumetric strains are 0.014 and 0.044 in Mg-PSZ and Ce-TZP, respectively. In addition to providing the materials of a controlled density and distribution of microcracks for acoustic studies of the stiffness matrix, the above deformation experiment was also used to measure the axial E and ν defined in Section II(3). More details of the experimental procedures are available elsewhere.[16]

(2) Pulse-Echo Technique

A standard pulse-echo technique using ultrasonic waves was employed to measure the elastic stiffness. The two zirconia materials, deformed to different volumetric strains, were cut into cubes with reference to the compression axis as shown in Fig. 2. The longitudinal and shear velocities were measured along all the cube directions. In the [100] direction, for example, two shear velocities, polarized along [010] and [001], need to be distinguished because of different symmetries. This is also indicated in Fig. 2. Velocities of five elastic waves were measured all together. The errors of these experiments were primarily due to the measurements of the dimensions and the parallelness of the cubic specimens. They were estimated to be within 0.2%. Of course, considerable variations of properties could still exist because of microstructural inhomogeneities due to transformation and damage, as we will indeed find to be the case later in Figs. 4 to 6.

The analysis of wave propagation in an elastic body is standard; hence, only results obtainable from standard references are given below. As mentioned previously, the symmetry in the present case is identical to that of a hexagonal crystal. Waves transmitted along the unique axis, [001], have the velocities given by

$$V_1 = V_{\text{longitudinal}} = (c_{33}/\rho)^{1/2} \quad \text{(along [001])}$$
$$V_2 = V_{\text{shear}} = (c_{44}/\rho)^{1/2} \quad \text{(along any transverse direction)} \tag{15}$$

For the [100] direction

$$V_3 = V_{\text{longitudinal}} = (c_{11}/\rho)^{1/2} \quad \text{(along [100])}$$
$$V_4 = V_{\text{shear}} = (c_{44}/\rho)^{1/2} \quad \text{(along [001])}$$
$$V_5 = V_{\text{shear}} = [(c_{11} - c_{12})/2\rho]^{1/2} \quad \text{(along [010])} \tag{16}$$

Measurements along these two directions will determine four of the five elastic constants. To determine the fifth one, a wave is transmitted along [101]. For the shear wave polarized along [010], the wave velocity is

$$V_6 = [(c_{11} - c_{12} + 2c_{44})/4\rho]^{1/2} \tag{17}$$

The nearly longitudinal wave and the other shear wave, polarized toward [101], suffer from acoustic birefringence. Their velocities are, respectively

$$V_{7,8} = [(A \pm B^{1/2})/2\rho]^{1/2} \tag{18}$$

where

$$A = (c_{11} + c_{33} + 2c_{44})/2$$
$$B = [(c_{11} - c_{33})/2]^2 + (c_{13} + c_{44})^2 \tag{19}$$

The density of the material, ρ, is given by

$$\rho = \rho^\circ/(1 + \varepsilon_v) \tag{20}$$

where ρ° is the initial density before deformation and ε_v is the volumetric plastic strain recorded during compression experiments.

In this study we have measured V_1 through V_5. Thus, all elastic constants except C_{13} have been determined.

IV. Experimental Results and Analysis

(1) Acoustic Measurements of Elastic Constants

Table I records the prior deformation history of the samples studied here. The measured wave velocities are presented in Table II. The calculated elastic constants are shown in Table III. We now discuss the results of Mg-PSZ and Ce-TZP separately.

(A) Mg-PSZ: Wave velocities and elastic constants of Mg-PSZ, recorded in Tables II and III, show considerable anisotropy from the compression axis to the transverse directions. Transverse isotropy was verified in all cases. Some direct insight into the stiffness matrix component can be obtained easily; for example, a lower velocity in the transverse direction corresponds to a c_{11} lower than c_{33}. In general, however, elastic constants have to be evaluated by converting wave velocities into c_{ij} using Eqs. (15) to (17) and Eq. (20). The data thus obtained are listed in Table III. The elastic constants normalized by those of the undeformed material, c_{ij}°, are plotted in Fig. 4. It is seen that the stiffness decreases monotonically with the fraction of transformation in the order of C_{44}, C_{33}, C_{66}, C_{11}, C_{12}, as predicted by the calculations. This is obvious by comparing Figs. 3 and 4. The assumption of transverse isotropy and an axial alignment of microcracks was thus verified.

To provide a quantitative comparison between the data and the model calculations and to infer the crack density, we renormalize the data as prescribed previously. The results are shown in Fig. 5. Apparently a linear dependence of stiffness evolution with the state variable is obeyed. To compare these data with Eqs. (10) and (12), we choose the following correla-

Table I. Plastic Strains of the Zirconia Specimens

Sample	$\varepsilon_{\text{axial}}$	$\varepsilon_{\text{radial}}$	ε_{vol}
Mg-PSZ			
1	−0.000 72	0.000 95	0.001 20
2	−0.004 55	0.006 56	0.008 57
3	−0.004 76	0.008 32	0.011 88
4	−0.007 65	0.010 91	0.014 17
Ce-TZP			
1	−0.008 25	0.010 85	0.013 45
2	−0.012 00	0.022 00	0.032 00
3	−0.027 40	0.035 50	0.043 60

Table II. Wave Velocities along Different Directions (m/s)

Sample	V_1	V_2	V_3	V_4	V_5
Mg-PSZ undeformed	7043.75	3724.80			
1	7028.46	3718.36	6956.11	3721.27	3735.61
2	6986.21	3729.87	6671.38	3731.62	3644.10
3	6987.61	3702.79	6647.23	3703.91	3647.26
4	6929.64	3662.09	6440.29	3680.21	3584.90
Ce-TZP undeformed	6634.12	3429.48			
1	6861.59	3441.50	6374.03	3708.69	3439.14
2	6913.58	3440.67	6398.61	3449.66	3563.43
3	5798.29	3140.97	4986.26	3127.03	3120.65

Table III. Stiffness Components for Deformed Zirconia (GPa)

Sample	ϕ	c_{11}	c_{12}	c_{33}	c_{44}	c_{66}
Mg-PSZ undeformed	0.000	282.30	124.41	282.30	78.94	78.94
1	0.085	274.83	116.31	280.57	78.53	79.26
2	0.605	251.09	101.25	275.35	78.48	74.92
3	0.834	248.46	98.85	274.56	77.03	74.80
4	1.000	232.70	88.49	267.93	74.84	72.11
Ce-TZP undeformed	0.000	272.43	126.83	272.43	72.80	72.80
1	0.309	248.15	103.66	287.56	82.05	72.25
2	0.734	245.57	93.24	286.69	71.01	76.17
3	1.000	147.47	31.94	199.41	58.71	57.77

tion between the crack density and the state variable:

$$\omega = 0.05\phi \tag{21}$$

in which the numerical coefficient in front of ϕ is treated as the only fitting parameter. With the above relationship, predictions of Eqs. (10) and (12), shown as the straight lines, are in close agreement with all four branches of the renormalized data.

The good agreement achieved by the use of only one adjustable parameter is nontrivial and lends us confidence in our model. In view of this, we believe that the crack density in deformed Mg-PSZ is now reasonably well established and correlates with the fraction of phase transformation according to Eq. (21). We further infer that even at $\omega = 0.05$, at the end of transformation plasticity, microcracks are essentially noninteracting so that their effects on the weakening of the stiffness matrix are additive, obeying a linear relationship with ω. Lastly, we may infer that the stiffness of an uncracked but transformed Mg-PSZ matrix is essentially isotropic.

(B) Ce-TZP: Data of Ce-TZP revealed an elastic anomaly in the early part of deformation and transformation. As can be seen from Tables II and III, wave velocities and stiffness constants in certain directions are higher than those of the undeformed Ce-TZP. This observation is clearly illustrated by the normalized elastic constants with reference to those of undeformed Ce-TZP, as plotted in Fig. 6. For example, at $\phi = 0.31$, the longitudinal and shear stiffnesses along the compressed [001] direction, C_{33} and C_{44}, have increased substantially. On the other hand, the longitudinal and shear stiffnesses along the transverse directions, C_{11} and C_{66}, have been depressed with reference to their later values at, e.g., $\phi = 0.73$. In the following paragraph and in Figs. 7 and 8 we digress to explore the origin of this anomaly. Readers interested in microcracking only may simply proceed to the paragraph after the next and to Fig. 9.

This elastic anomaly may be attributed to the transformation texture which has been documented by Li *et al.*[19] and Bowman *et al.*[20] for tetragonal polycrystals deformed under similar conditions. Essentially, while the undeformed Ce-TZP has a random texture consisting of the tetragonal phase only, the stress-assisted transformation strongly favors those tetragonal variants with the maximum shear coupling between the applied stress and the transformation strain, as schematically indicated by Fig. 7. This in turn, as shown by the above

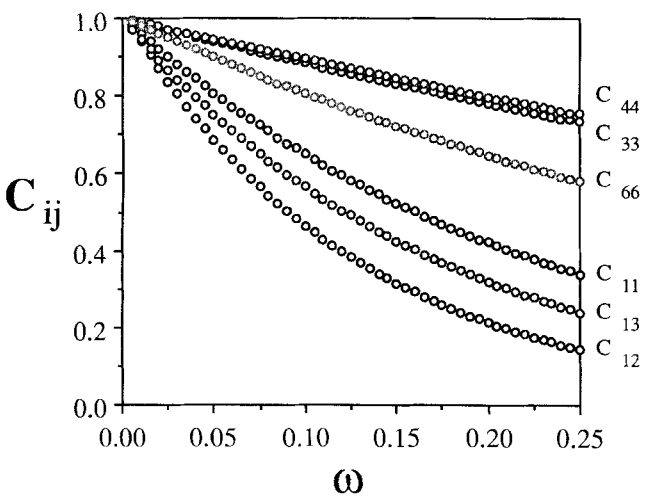

Fig. 3. Normalized elastic stiffness matrix components as a function of the normalized crack density.

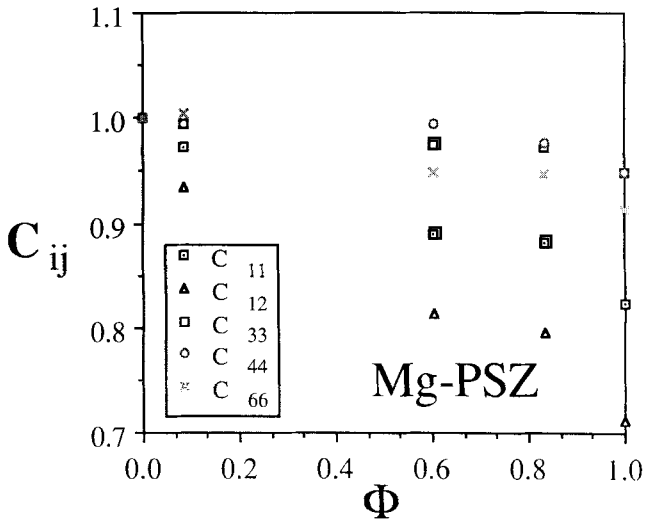

Fig. 4. Normalized elastic stiffness of a deformed Mg-PSZ.

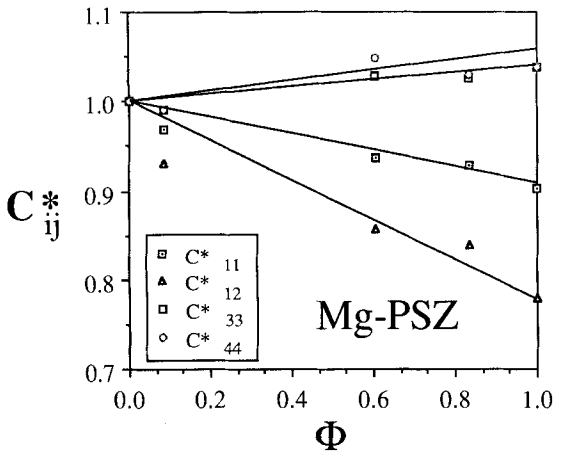

Fig. 5. Renormalized elastic stiffness, by C_{66}, of a deformed Mg-PSZ. The straight lines are model predictions given by Eqs. (10) and (12), by setting $\omega = 0.05\phi$.

authors, leads to a texture of both the transformed monoclinic phase and the remaining untransformed tetragonal phase. The resultant texture of the deformed Ce-TZP follows a simple pattern; namely, the remaining tetragonal crystals tend to have their longer axes [002] aligned perpendicular to the compression axis, and, correspondingly, the transformed monoclinic crystals tend to have their longer axes $[11\bar{1}]/[\bar{1}11]$ aligned in the same way. This can be seen in Fig. 8, in which the X-ray diffraction patterns of a uniaxially compressed Ce-TZP are shown for the axial and radial cross sections. From a simple bonding consideration, the shorter crystal axis is expected to have a higher longitudinal and shear stiffness than the longer crystal axis. Thus, both the remaining tetragonal and the newly formed monoclinic crystals may be expected to be "stiffer" in the compression direction than in the transverse direction. This was precisely what we observed in Fig. 6 at low ϕ.

Regardless of this elastic anomaly at earlier stages, eventually, at full transformation, $\phi = 1.0$, the stiffness constants are again weakened in the same order predicted by the model calculations. Although a precise, quantitative comparison with our model calculations is no longer warranted because of the presence of elastic anisotropy of the reference solid, this terminal behavior strongly implies that the microcracks in Ce-TZP are also aligned axially. A rough comparison of these data with the model calculations placed an estimate of the crack density at $\phi = 1.0$ to be between 0.1 and 0.15, i.e., 2 to 3 times the amount in Mg-PSZ. We regard this reasonable in view of their respective volume fractions of the transformable phase.

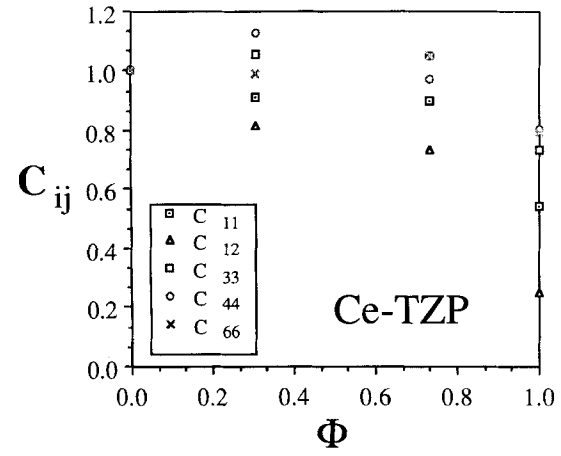

Fig. 6. Normalized elastic stiffness of a deformed Ce-TZP. Note the initial rise of C_{33} and C_{44}.

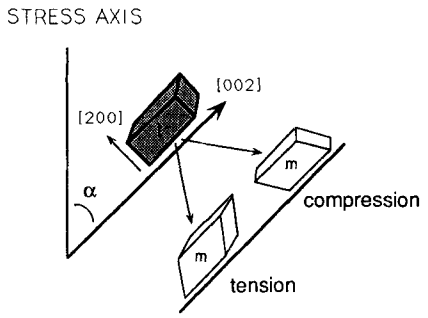

Fig. 7. Relationship between applied stress in axisymmetric deformation and the *t*-to-*m* transformation. The tetragonality in the *t* phase is greatly exaggerated.

(2) Axial E and ν

Our acoustic measurements confirmed that transformation plasticity is accompanied by microcracking, which has a strongly nonisotropic orientation distribution dictated by the stress state. In compression, microcracks are aligned along the stress axis but otherwise possess transverse isotropy. To provide an independent verification of the above picture, we now turn to the other prediction of the elasticity model that Young's modulus and Poisson's ratio along the compression axis remain unchanged. A direct verification of the latter prediction is possible since, in triaxial compression testing of zirconia, the instantaneous elastic properties can be monitored along the way in the axial and radial directions by intermittent unloading–loading cycles during plastic deformation. The linear portions of the loading and unloading stress–strain curves in the axial and radial directions could then be used to compute Young's modulus and Poisson's ratio for the axial loading. (The friction due to the O-ring in the pressure vessel was taken into account in analyzing unloading–loading stress strain curves. In addition, at higher fractions of transformation, Young's modulus was measured after reinitiation of loading (or unloading) following a stress relaxation period. In this way, the relaxation effects due to transformation or frictional sliding of crack faces could be avoided. The errors of these experiments, though larger than conventional elastic moduli measurements, were estimated to be within ±3%. The related details of the test procedure are given elsewhere.[16])

Young's modulus E and Poisson's ratio ν for Mg-PSZ and Ce-TZP for axial deformation measured by the above method are shown in Fig. 9. It was found that, within the precision of the present experiment, Young's modulus and Poisson's ratio for axial loading remain unchanged throughout the progression of transformation plasticity, except for a small rise initially in E in Ce-TZP which is associated with the elastic anomaly discussed previously. This is, indeed, the result predicted in Section II(3) if microcracks are aligned along the stress axis. Thus the picture of axial cracks is reconfirmed.

V. Discussion

(1) Transformation Plasticity

Since microcracking is proportional to the fraction of transformation, as inferred from Fig. 5, the volumetric strain measured in our study contains two proportional contributions from the transformation and microcracking. The latter, estimated as $\omega\delta/2a$, where δ is the wedge opening depicted in Fig. 1, is primarily manifested as a radial strain in our experiment. Using reasonable microstructural parameters, this contribution was found to be relatively small. Thus the volume strain arises almost entirely from the phase transformation. This provides, *a posteriori*, a justification of the use of ϕ as a state variable in our study.

We noted that the transformation texture imparts a strong anisotropy into the elastic properties of the deformed Ce-TZP.

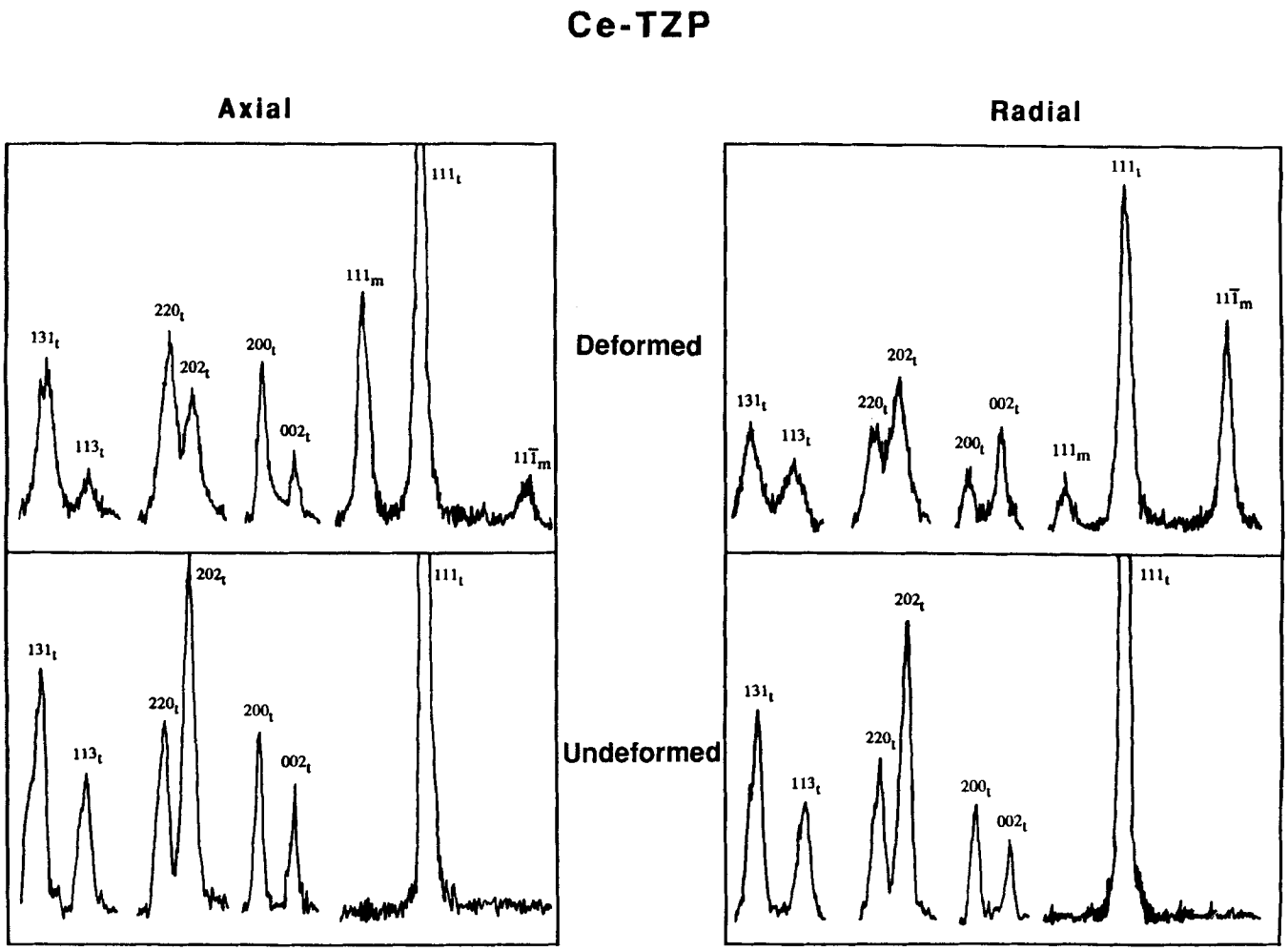

Fig. 8. X-ray diffraction patterns of Ce-TZP before and after uniaxial compression. The axial cross section is normal to the compression stress axis.

The elastic anisotropy arises from both the remaining tetragonal phase and the newly formed monoclinic phase. Such an effect is probably unimportant in the Mg-PSZ because the latter, unlike Ce-TZP, is comprised largely of an untransformable (cubic) matrix, with only 33 vol% of transformable tetragonal precipitates. As such, the reference uncracked but transformed Mg-PSZ is largely isotropic and apparently satisfies Eq. (11). It is plausible that this distinction between Mg-PSZ and Ce-TZP can be generalized to other zirconia systems of similar microstructures.

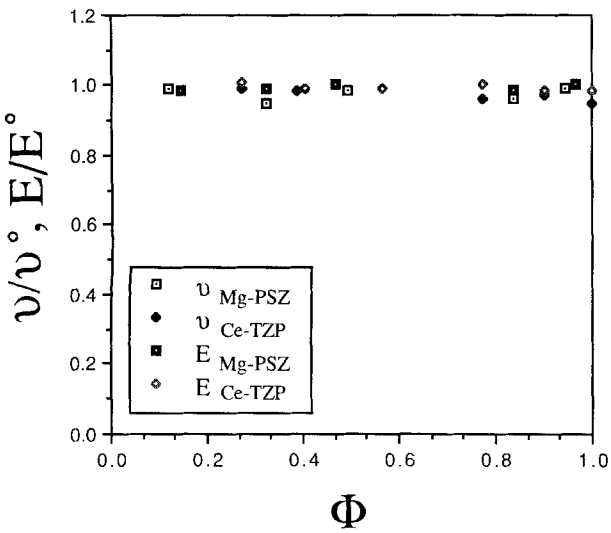

Fig. 9. Normalized Young's modulus and Poisson's ratio for Mg-PSZ and Ce-TZP for axial deformation.

(2) Microcracking in Tension

As pointed out in the Introduction, elastic anisotropy due to a nonrandom distribution of microcracks is a common feature in deformed brittle ceramics. In addition to the compression symmetry studied above, creep damage can produce the tension symmetry depicted in Fig. 1(a). Unlike the compression case, in which only the axial moduli E and ν are unaltered, the tension symmetry with microcracks perpendicular to the tensile axis has only two moduli altered. These are the axial Young's modulus $E = (s_{33})^{-1}$ and the axial shear rigidity $G = (s_{44})^{-1} = (s_{55})^{-1}$ given by

$$E = E^\circ[1 - 16(1 - \nu^2)\omega/3] \tag{22}$$

$$G = G^\circ\{1 - 16[(1 - \nu)/(2 - \nu)]\omega/3\} \tag{23}$$

in the dilute crack density limit.[10,21] In the above, E° and G° are Young's modulus and the shear rigidity of the uncracked reference solid. The stiffness matrix can be easily derived from the above. Since crept specimens in tension are increasingly available in recent years, it should be interesting to attempt to verify the above prediction in the future.

Microcracking due to transformation plasticity, subject to a predominantly tensile stress field, is of relevance to the

strength of transformation-toughened ceramics. In some highly transformable, very high toughness zirconia, preexisting flaws are not capable of initiating fracture. In turn, the tensile strength is found to be limited by the tensile yield stress.[22] We have previously proposed that the strength-limiting factor in this case is the rampant formation of microcracks.[7] Indeed, two zirconias studied here have evidenced a drastic stiffness reduction once transformation is complete in bulk specimens. It should be noted that when macroscopic yielding occurs, transformation plasticity is actually spatially inhomogeneous on a finer scale. Because of autocatalysis and shear localization which tends to accompany transformation plasticity in zirconia ceramics,[7,16-18] the local damage can be severe and comparable to the one observed here for fully transformed bulk materials. Furthermore, all the microcracks formed in tensile deformation are normal to the stress axis and capable of resulting in an even more severe loss of load-carrying capability. Thus, in highly transformable zirconia loaded to the macroscopic yield stress, the localized initiation of transformation plasticity will probably be accompanied by a fatal microcrack damage which is unsustainable under the tensile yield stress and must cause a localized, catastrophic propagation of yield and fracture. This is probably the cause of yield limited strength behavior first noted by Swain.[22]

VI. Conclusion

(1) Under triaxial compression, Mg-PSZ and Ce-TZP develop a high density of transformation-induced microcracks which are uniformly distributed and parallel to the compression axis.

(2) Because of the relatively small volume fraction of the transformable phase, deformed Mg-PSZ remains largely isotropic in crystallographic texture. Axial microcracks cause anisotropic weakening in stiffness in the order of $C_{44}, C_{33}, C_{66}, C_{11}, C_{13}, C_{12}$ in quantitative agreement with the prediction of the elasticity theory. The terminal crack density Na^3 reaches 0.05 in Mg-PSZ. Even at such density interactions among microcracks appears insignificant.

(3) A strong transformation texture of both the transformed monoclinic phase and the remaining tetragonal phase develops in Ce-TZP, causing an initial strengthening in the axial direction. In the end, as transformation progresses, axial microcracks begin to have a dominant weakening effect on stiffness in the way predicted by the theory. The terminal crack density exceeds 0.1 in Ce-TZP.

(4) In view of the very high crack density and very severe elastic degradation associated with the stress-assisted transformation in both Mg-PSZ and Ce-TZP, strength of transformation-toughened zirconia ceramics is ultimately limited by the tensile yield (transformation) stress.

Acknowledgments: We thank Dr. K. J. Bowman and Mr. J. Hall for their assistance in preparing this manuscript.

References

[1]F. J. P. Clarke, "Residual Strain and Fracture Stress–Grain Size Relationship in Brittle Solids," *Acta Metall.*, **12** [2] 139–43 (1964).

[2]R.W. Davidge, "Cracking at Grain Boundaries in Polycrystalline Brittle Materials," *Acta Metall.*, **29**, 1695–702 (1981).

[3]J. B. Walsh, "The Effect of Cracks on the Compressibility of Rock," *J. Geophys. Res.*, **70** [2] 381–89 (1965).

[4]B. Budiansky and R. J. O'Connell, "Elastic Moduli of a Cracked Solid," *Int. J. Solids Struct.*, **12**, 81–97 (1976).

[5]W. F. Brace, B.W. Paulding, Jr., and C. Scholz, "Dilatancy in the Fracture of Crystalline Rocks," *J. Geophys. Res.*, **71** [16] 3939–54 (1966).

[6]J. P. Porter, W. Blumenthal, and A.G. Evans, "Creep Fracture in Ceramic Polycrystals—I. Creep Cavitation Effects in Polycrystalline Alumina," *Acta Metall.*, **29**, 1899–906 (1981).

[7]I-W. Chen and P. E. Reyes-Morel, "Implications of Transformation Plasticity in ZrO_2-Containing Ceramics: I, Shear and Dilatation Effects," *J. Am. Ceram. Soc.*, **69** [3] 181–89 (1986).

[8]C. Zener, "Micro Mechanism of Fracture"; pp. 3–31 in Fracturing of Metals. American Society for Metals, Metals Park, OH, 1949.

[9]A. N. Stroh, "A Theory of the Fracture of Metals," *Adv. Phys.*, **6**, 418–65 (1957).

[10]A. Hoenig, "Elastic Moduli of a Non-Randomly Cracked Body," *Int. J. Solids Struct.*, **15**, 137–54 (1979).

[11]J. B. Walsh, "The Effect of Cracks on the Uniaxial Elastic Compression of Rocks," *J. Geophys. Res.*, **70** [2] 399–411 (1965).

[12]A. G. Evans and K.T. Faber, "Crack-Growth Resistance of Microcracking Brittle Materials," *J. Am. Ceram. Soc.*, **67** [4] 255–60 (1984).

[13]L. Ewart and S. Suresh, "Dynamic Fatigue Crack Growth in Polycrystalline Alumina Under Cyclic Compression," *J. Mater. Sci. Lett.*, **5**, 774–78 (1986).

[14]M. P. Cleary, I-W. Chen, and S. M. Lee, "Self-Consistent Techniques for Heterogeneous Media," *J. Eng. Mech. Div., Am. Soc. Civ. Eng.*, **106**, 861–87 (1980).

[15]P. E. Reyes-Morel, J. S. Cherng, and I-W. Chen, "Transformation Plasticity of Ce-TZP: II, Pseudoelasticity and Shape Memory Effect," *J. Am. Ceram. Soc.*, **71** [8] 648–51 (1988).

[16]P. E. Reyes-Morel, "An Experimental Study of Constitutive Relations of Transformation Plasticity in Zirconia-based Ceramics"; Ph.D. Thesis. Massachusetts Institute of Technology, Cambridge, MA, 1986.

[17]P. E. Reyes-Morel and I-W. Chen, "Transformation Plasticity of Ce-TZP: I, Stress Assistance and Autocatalysis," *J. Am. Ceram. Soc.*, **71** [6] 343–53 (1988).

[18]I-W. Chen and P. E. Reyes-Morel, "Transformation Plasticity and Transformation Toughening in Mg-PSZ and Ce-TZP"; pp. 75–88 in Advanced Structural Ceramics. Edited by P. F. Becher, M.V. Swain, and S. Somiya. Materials Research Society Symposium Series, Materials Research Society, Pittsburgh, PA, 1986.

[19]B-S. Li, J-S. Cherng, K. J. Bowman, and I-W. Chen, "Domain Switching as a Toughening Mechanism in Tetragonal Zirconia," *J. Am. Ceram. Soc.*, **71** [7] C-362–C-364 (1988).

[20]K. J. Bowman, P. E. Reyes-Morel, and I-W. Chen, "Texture from Deformation of Zirconia-Containing Ceramics"; pp. 811–16 in Proceedings of the Eighth International Conference on Texture of Materials (ICOMAT 8). Edited by J. S. Kallend and G. Gottstein. The Metallurgical Society, Warrendale, PA, 1988.

[21]D. P. H. Hasselman and J. P. Singh, "Analysis of Thermal Stress Resistance of Microcracked Brittle Ceramics," *Am. Ceram. Soc. Bull.*, **56** [6] 559–62 (1979).

[22]M.V. Swain, "Inelastic Deformation of Mg-PSZ and its Significance for Strength–Toughness Relationship of Zirconia Toughened Ceramics," *Acta Metall.*, **33** [11] 2083–91 (1985). □